ARTICLE

One-Shot Simulation of Static Disorder in Quantum Dynamics with Equilibrium Initial State via Matrix Product State Sampling†

Zhao Zhang, Jiajun Ren*, Wei-Hai Fang

Key Laboratory of Theoretical and Computational Photochemistry, Ministry of Education, College of Chemistry, Beijing Normal University, Beijing 100875, China

(Dated: Received on June 8, 2025; Accepted on July 15, 2025)

Static disorder plays a crucial role in the electronic dynamics and spectroscopy of complex molecular systems. Traditionally, obtaining observables averaged over static disorder requires thousands of realizations via direct sampling of the disorder distribution, leading to high computational costs. In this work, we extend the auxiliary degree-of-freedom based matrix product state (MPS) method to handle system-bath correlated thermal equilibrium initial states, which can capture static disorder effects using a one-shot quantum dynamical simulation. We validate the effectiveness of the extended method by computing the dipole–dipole time correlation function of the Holstein model relevant to the emission spectrum of molecular aggregates. Our results show that the one-shot method is very accurate with only a moderate increase in MPS bond dimension, thereby significantly reducing computational cost. Moreover, it enables the generation of a much larger number of samples than the conventional direct sampling method at negligible additional cost, thus reducing statistical errors. This method provides a broadly useful tool for calculating equilibrium time correlation functions in system-bath coupled models with static disorder.

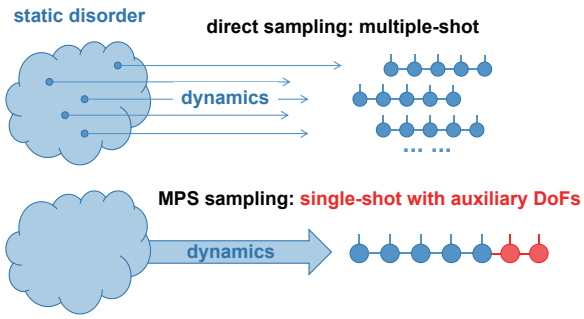

Key words: Matrix product state, Static disorder, Quantum dynamics, Time correlation function

I. INTRODUCTION

Static disorder, arising from defects, structural fluctuations, or packing imperfections, can have a profound influence on electronic dynamics and spectroscopy in molecular aggregates and materials, such as charge and exciton migration, transport, and relaxation processes [1–10]. In theoretical modeling, static disorder is typically represented by distributions in local site energies or electronic couplings, often assumed to follow a Gaussian distribution [3, 11–14] or other distributions, such as Lorentzian and Lévy distributions [15, 16]. To calculate observables averaged over static disorder, one typically sample a large number of disorder realizations and perform independent simulations for each. When each realization involves computationally intensive simulations, such as full quantum dynamics, the overall cost becomes prohibitively high, even though these simulations are perfectly parallelizable.

To address this challenge, in 2021, Gelin *et al.* proposed an auxiliary degree-of-freedom (DoF) approach that incorporates static disorder into a single quantum

† Part of Special Topic "Quantum Dynamics in Complex Systems".

* Author to whom correspondence should be addressed.
E-mail: jjren@bnu.edu.cn

 © 2025 Chinese Physical Society

dynamical simulation [17], thereby eliminating the need for averaging over thousands of realizations. When combined with efficient time-dependent matrix product state (MPS) algorithms [18], this method has been successfully applied to simulate static disorder effects in charge transfer dynamics within the Holstein-Peierls model [17], and energy transport in the eight-site Fenna-Matthews-Olson model [19]. However, the original auxiliary-DoF-based approach cannot handle system-bath correlated initial state at thermal equilibrium, which depends on the static disorder itself. Such a correlated equilibrium state are crucial for calculating equilibrium time correlation functions and dynamical response properties in system-bath coupled systems [20].

To overcome this limitation, in this work, we propose a new MPS-sampling algorithm that extends the auxiliary-DoF method to handle static-disorder-dependent thermal equilibrium initial states. We demonstrate the validity of our approach by calculating the dipole–dipole time correlation function of the Holstein model under varying disorder strengths and system sizes. Our method achieves comparable accuracy to the standard direct sampling approach, but with only a one-shot simulation, leading to significant savings in computational cost.

The remainder of this paper is organized as follows. Section II presents the detailed algorithm. Section III provides numerical examples comparing our MPS-sampling approach with the traditional direct sampling approach. Finally, conclusions are summarized in Section IV.

II. METHOD

A. Static disorder

We focus on the calculation of quantum two-time correlation functions (TCFs) $\langle\hat{A}(t)B\rangle$. This quantity reduces to the time-dependent expectation value of a single observable $\langle\hat{A}(t)\rangle$ when $\hat{B}=\hat{I}$, and it can be naturally generalized to multi-time correlation functions.

In the presence of static disorder, the TCF becomes

$$\langle\hat{A}(t)\hat{B}\rangle=\int\langle\hat{A}(\mathbf{s},t)\hat{B}(\mathbf{s})\rangle\rho(\mathbf{s})\mathrm{d}\mathbf{s}. \tag{1}$$

For a pure initial state,

$$\langle\hat{A}(\mathbf{s},t)\hat{B}(\mathbf{s})\rangle=\langle\psi(\mathbf{s},0)|\mathrm{e}^{i\hat{H}(\mathbf{s})t}\hat{A}(\mathbf{s})\mathrm{e}^{-i\hat{H}(\mathbf{s})t}\hat{B}(\mathbf{s})|\psi(\mathbf{s},0)\rangle \tag{2}$$

For a thermal equilibrium initial state,

$$\langle\hat{A}(\mathbf{s},t)\hat{B}(\mathbf{s})\rangle=\mathrm{Tr}\left[\frac{\mathrm{e}^{-\beta\hat{H}(\mathbf{s})}}{Z(\mathbf{s})}\mathrm{e}^{i\hat{H}(\mathbf{s})t}\hat{A}(\mathbf{s})\mathrm{e}^{-i\hat{H}(\mathbf{s})t}\hat{B}(\mathbf{s})\right]. \tag{3}$$

$\mathbf{s}=\{s_1,s_2,\cdots\}$ represents the parameters characterizing static disorder (*e.g.*, fluctuation in site energies), and $\rho(\mathbf{s})$ is their probability distribution, satisfying $\rho(\mathbf{s})>0$ and $\int\rho(\mathbf{s})\mathrm{d}\mathbf{s}=1$. The Hamiltonian $\hat{H}$, the observables $\hat{A}$ and $\hat{B}$, and the initial state all depend on $\mathbf{s}$ in general.

The standard approach to calculate Eq.(1) is through Monte Carlo sampling of $\mathbf{s}$ according to $\rho(\mathbf{s})$.

$$\langle\hat{A}(t)\hat{B}\rangle\approx\frac{1}{N_{\mathrm{samp}}}\sum_{k=1}^{N_{\mathrm{samp}}}\langle\hat{A}(\mathbf{s}_k,t)\hat{B}(\mathbf{s}_k)\rangle \tag{4}$$

We refer to this as the direct sampling method. It requires a large number of independent quantum dynamics simulations, leading to high computational cost. The statistical error in this method scales as $1/\sqrt{N_{\mathrm{samp}}}$, where N_{samp} is the number of samples.

B. Auxiliary-DoF-based method with static-disorder-independent initial states

To reduce the high computational cost of direct sampling, Gelin *et al.* proposed a novel algorithm in which auxiliary DoFs, $\mathbf{s}$, were introduced into the quantum system [17]. The wavefunction of the auxiliary DoFs, $\chi(\mathbf{s})$, is chosen such that $\chi^*(\mathbf{s})\chi(\mathbf{s})=\rho(\mathbf{s})$, allowing the effect of disorder to be encoded into a single simulation.

In the original formulation, $\rho(\mathbf{s})$ was assumed to be Gaussian,

$$\rho(\mathbf{s})=\prod_i\rho(s_i) \tag{5}$$

$$\rho(s_i)=\frac{1}{\sqrt{2\pi}\sigma}\mathrm{e}^{-{s_i}^2/(2\sigma^2)} \tag{6}$$

Thus, $\chi(\mathbf{s})$ is naturally the ground state wavefunction of harmonic oscillators, which is

$$\chi(\mathbf{s})=\prod_i\chi_0(s_i) \tag{7}$$

$$\chi_0(s_i)=\left(\frac{\omega}{\pi}\right)^{1/4}\mathrm{e}^{-1/2[{s_i}^2/(1/\omega)]}. \tag{8}$$

To satisfy $|\chi_0(s_i)|^2=\rho(s_i)$, the frequency of the oscilla-

DOI: 10.1063/1674-0068/cjcp2506080
© 2025 Chinese Physical Society

tor is chosen as $\omega = 1/(2\sigma^2)$.

In this work, we generalize this formulation to arbitrary static disorder distributions by working in the "coordinate space" rather than the bosonic Fock space used in the original method. We define the auxiliary wavefunction as

$$|\chi\rangle = \int \mathrm{d}\mathbf{s}\sqrt{\rho(\mathbf{s})}|\mathbf{s}\rangle. \tag{9}$$

Accordingly, the static disorder related parameters in the Hamiltonian becomes operators of the auxiliary DoFs, which behave like coordinate operators and fullfills

$$\hat{s}_i|s_i\rangle = s_i|s_i\rangle. \tag{10}$$

For example, to describe the static energetic disorder of local electronic state,

$$\hat{H}(\mathbf{s}) = \sum_i (\varepsilon_0 + s_i)|\phi_i\rangle\langle\phi_i|, \qquad s_i \sim \rho_i(s_i) \tag{11}$$

$$\rightarrow \hat{H}(\hat{\mathbf{s}}) = \sum_i (\varepsilon_0 + \hat{s}_i)|\phi_i\rangle\langle\phi_i|. \tag{12}$$

If the initial state is independent of static disorder, *i.e.*, $\psi(\mathbf{s},0) \equiv \psi(0)$, Eq.(1) can be simplified to

$$\langle\hat{A}(t)B\rangle = \langle\chi|\langle\psi(0)|\hat{A}(\hat{\mathbf{s}},t)\hat{B}(\hat{\mathbf{s}})|\psi(0)\rangle|\chi\rangle \tag{13}$$

$$|\chi\rangle = \prod_i |\chi_i\rangle \tag{14}$$

With this auxiliary-DoF-based method, only one single quantum dynamics simulation from the initial state $|\Psi(0)\rangle = |\psi(0)\rangle|\chi\rangle$ is needed to obtain the static-disorder-averaged quantity, with the trade-off being the inclusion of additional auxiliary DoFs, which enlarge the Hilbert space.

In practice, the continuous variables $\hat{\mathbf{s}}$ must be discretized. This can be done using either a harmonic oscillator basis (as in Refs. [17, 19]) or a discrete variable representation (DVR) [21, 22], as employed in this work. With a sufficiently large basis size, the results converge to the continuum limit. The auxiliary-DoF-based method can be effectively combined with time-dependent algorithms based on tensor network states, such as time-dependent density matrix renormalization group (TD-DMRG) [23–30] or multilayer multi-configurational time-dependent Hartree (ML-MCTDH) [31–35]. The additional computational cost due to auxiliary DoFs is usually expected to be negligible. Here, we discuss qualitatively when this expectation is reasonable. In the auxiliary-DoF-based method, the overall time-evolved wavefunction $\Psi(t)$ is actually a linear combination of all the wavefunctions, each with specific static disorder $\mathbf{s}$ weighted by $\sqrt{\rho(\mathbf{s})}$

$$\Psi(t) = \int \mathrm{d}\mathbf{s}\sqrt{\rho(\mathbf{s})}|\psi(\mathbf{s},t)\rangle|\mathbf{s}\rangle \tag{15}$$

$$\psi(\mathbf{s},t) = \mathrm{e}^{-i\hat{H}(\mathbf{s})t}\psi(0) \tag{16}$$

If the individual wavefunctions $|\psi(\mathbf{s},t)\rangle$ are similar across $\mathbf{s}$, then the combined wavefunction can be efficiently compressed by tensor network algorithms. This condition holds when the static disorder is moderate, and thus the disorder does not significantly alter the wavefunction.

It should be noted that the above method is not limited to static disorder of local energy, it can be directly used to handle other types of static disorders, such as that of excitonic coupling terms,

$$\hat{H}(\mathbf{s}) = \sum_{ij} (J^0_{ij} + s_{ij})|\phi_i\rangle\langle\phi_j|, \qquad s_{ij} \sim \rho_{ij}(s_{ij}) \tag{17}$$

$$\rightarrow \hat{H}(\hat{\mathbf{s}}) = \sum_{ij} (J^0_{ij} + \hat{s}_{ij})|\phi_i\rangle\langle\phi_j|, \tag{18}$$

where s_{ij} represents the static disorder of excitonic coupling between state i and state j. Moreover, this method can handle a broad range of system-bath interactions, provided the interaction can be expressed in a sum-of-products form $\sum_i \lambda_i \hat{S}_i \otimes \hat{B}_i$, which is always fulfilled for model Hamiltonians. This flexibility arises because the underlying TD-DMRG method treats the full system-bath composite as a closed quantum system, rather than relying on reduced dynamics approaches that often assume specific forms of interaction, such as linear system-bath interactions.

Despite its advantage, this method is limited to static-disorder-independent initial states. For thermal correlation functions starting from a system-bath correlated equilibrium state (Eq.(3)), the initial state depends on $\mathbf{s}$ itself. To overcome this limitation, we have developed a new auxiliary-DoF-based MPS-sampling method.

C. Auxiliary-DoF-based MPS-sampling method for static-disorder-dependent thermal equilibrium initial states

We now describe how to extend the auxiliary-DoF

DOI: 10.1063/1674-0068/cjcp2506080 © 2025 Chinese Physical Society

approach to thermal equilibrium initial states that depend on static disorder, using the purification method in combination with sampling MPS.

In the purification method, an auxiliary space Q is introduced (distinct from the auxiliary DoFs representing disorder). This allows the mixed thermal state in the physical space P to be represented as a pure state $|\psi\rangle$ in the enlarged space $P\otimes Q$, satisfying $\rho_P=\mathrm{Tr}_Q|\psi\rangle\langle\psi|$ [36, 37].

At an infinitely high temperature ($\beta=0$), the purified thermal state $|\psi_{\beta=0}\rangle$ is trivially known,

$$|\psi_{\beta=0}\rangle=\sum_{\sigma,\tilde{\sigma},\sigma=\tilde{\sigma}}\frac{1}{\sqrt{d^N}}|\sigma_1\tilde{\sigma}_1\sigma_2\tilde{\sigma}_2\cdots\sigma_N\tilde{\sigma}_N\rangle, \tag{19}$$

fulfilling $\rho_{\mathrm{eq}}(\beta=0)=\mathrm{Tr}_Q|\psi_{\beta=0}\rangle\langle\psi_{\beta=0}|=\hat{I}/d^N$, where d is the dimension of the local Hilbert space of one DoF, and N is the number of physical DoFs. The state $|\psi_{\beta=0}\rangle$ can be represented as an MPS with a maximum bond dimension $M=d$ (or as a matrix product operator with $M=1$) [28]. The thermal state at a finite temperature is then obtained via imaginary-time evolution from $\tau=0$ to $\tau=\beta/2$.

$$|\psi_\beta\rangle=\frac{\mathrm{e}^{-\beta\hat{H}/2}|\psi_{\beta=0}\rangle}{\sqrt{\langle\psi_{\beta=0}|\mathrm{e}^{-\beta\hat{H}/2}\mathrm{e}^{-\beta\hat{H}/2}|\psi_{\beta=0}\rangle}} \tag{20}$$

The desired TCF is obtained from subsequent real-time evolution.

$$\langle\hat{A}(t)\hat{B}\rangle=\frac{\langle\psi_{\beta=0}|\mathrm{e}^{-\beta\hat{H}/2}\hat{A}(t)\hat{B}\mathrm{e}^{-\beta\hat{H}/2}|\psi_{\beta=0}\rangle}{\langle\psi_{\beta=0}|\mathrm{e}^{-\beta\hat{H}/2}\mathrm{e}^{-\beta\hat{H}/2}|\psi_{\beta=0}\rangle}. \tag{21}$$

With static disorder, Eq.(21) becomes

$$\langle\hat{A}(t)\hat{B}\rangle=\langle\chi|\frac{\langle\psi_{\beta=0}|\mathrm{e}^{-\beta\hat{H}(\hat{\mathbf{s}})/2}\hat{A}(\hat{\mathbf{s}},t)\hat{B}(\hat{\mathbf{s}})\mathrm{e}^{-\beta\hat{H}(\hat{\mathbf{s}})/2}|\psi_{\beta=0}\rangle}{\langle\psi_{\beta=0}|\mathrm{e}^{-\beta\hat{H}(\hat{\mathbf{s}})/2}\mathrm{e}^{-\beta\hat{H}(\hat{\mathbf{s}})/2}|\psi_{\beta=0}\rangle}|\chi\rangle \tag{22}$$

This cannot be evaluated simply by evolving $|\psi_{\beta=0}\rangle\otimes|\chi\rangle$, which would yield an incorrect result.

$$\frac{\langle\chi|\langle\psi_{\beta=0}|\mathrm{e}^{-\beta\hat{H}(\hat{\mathbf{s}})/2}\hat{A}(\hat{\mathbf{s}},t)\hat{B}(\hat{\mathbf{s}})\mathrm{e}^{-\beta\hat{H}(\hat{\mathbf{s}})/2}|\psi_{\beta=0}\rangle|\chi\rangle}{\langle\chi|\langle\psi_{\beta=0}|\mathrm{e}^{-\beta\hat{H}(\hat{\mathbf{s}})/2}\mathrm{e}^{-\beta\hat{H}(\hat{\mathbf{s}})/2}|\psi_{\beta=0}\rangle|\chi\rangle}\neq\langle\hat{A}(t)\hat{B}\rangle \tag{23}$$

To address this, we calculate three intermediate states, each of which is represented as an MPS,

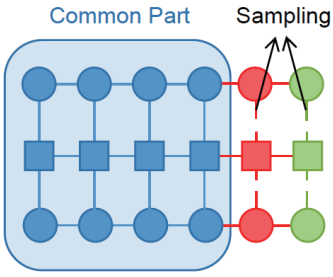

FIG. 1 Contraction diagram of $\langle\Psi_L(\mathbf{s}_k)|\hat{A}(\mathbf{s}_k)|\Psi_R(\mathbf{s}_k)\rangle$ using matrix product states (MPS) and matrix product operator (MPO). The blue part represents the degrees of freedom shared across all samples $\mathbf{s}_k$ and can be reused. The red and green part correspond to the auxiliary degrees of freedom associated with static disorder, which are sampled to generate $\mathbf{s}_k$. The calculation of $\langle\Psi_\beta(\mathbf{s}_k)|\Psi_\beta(\mathbf{s}_k)\rangle$ follows a similar contraction structure.

$$|\Psi_\beta\rangle=\mathrm{e}^{-\beta\hat{H}(\hat{\mathbf{s}})/2}|\psi_{\beta=0}\rangle|\chi\rangle \tag{24}$$

$$|\Psi_L\rangle=\mathrm{e}^{-i\hat{H}(\hat{\mathbf{s}})t}|\Psi_\beta\rangle \tag{25}$$

$$|\Psi_R\rangle=\mathrm{e}^{-i\hat{H}(\hat{\mathbf{s}})t}\hat{B}(\hat{\mathbf{s}})|\Psi_\beta\rangle \tag{26}$$

Then, according to the discretized distribution function $\rho(\mathbf{s})$, we sample a set of configurations $\mathbf{s}_k$. For each $\mathbf{s}_k$, we extract: $|\Psi_\beta(\mathbf{s}_k)\rangle$, $|\Psi_L(\mathbf{s}_k)\rangle$, $|\Psi_R(\mathbf{s}_k)\rangle$ and $\hat{A}(\mathbf{s}_k)$. Eq.(22) is then computed as:

$$\langle\hat{A}(t)\hat{B}\rangle=\frac{1}{N_{\mathrm{samp}}}\sum_{\mathbf{s}_k}\frac{\langle\Psi_L(\mathbf{s}_k)|\hat{A}(\mathbf{s}_k)|\Psi_R(\mathbf{s}_k)\rangle}{\langle\Psi_\beta(\mathbf{s}_k)|\Psi_\beta(\mathbf{s}_k)\rangle} \tag{27}$$

We call this the auxiliary-DoF-based MPS-sampling method. Each term of Eq.(27) can be computed via efficient tensor contractions. Since for different $\mathbf{s}_k$, the contraction is largely the same except for the sites corresponding to static disorder, intermediate contractions can be cached and reused at each time step (as illustrated in FIG. 1). In addition, the denominator (partition function) is time-independent and thus computed only once.

Although this method involves sampling, it differs from direct sampling. All sampled terms are extracted from a single time-evolved MPS that includes auxiliary DoFs, rather than from many independent simulations. This can significantly reduce computational cost. As in the previous subsection, the effectiveness of the method depends on the similarity of wavefunctions for different $\mathbf{s}_k$. Encouragingly, in our numerical tests, the MPS representation remains efficient when the disorder strength is not excessively large.

DOI: 10.1063/1674-0068/cjcp2506080
© 2025 Chinese Physical Society

III. RESULTS AND DISCUSSION

We benchmark the auxiliary-DoF-based MPS-sampling method by calculating the dipole–dipole time correlation function, $\langle\hat{\mu}(t)\hat{\mu}\rangle$, for the emission spectrum of a one-dimensional Holstein model with static disorder at a finite temperature. The Holstein model is widely used to describe excited-state dynamics and spectroscopy in molecular aggregates and materials [3, 38–40]. The Hamiltonian including diagonal static disorder is

$$\hat{H}=\sum_i(\varepsilon_0+s_i)|\phi_i\rangle\langle\phi_i|+\sum_i J(|\phi_i\rangle\langle\phi_{i+1}|+|\phi_{i+1}\rangle\langle\phi_i|)+\sum_i g\omega(b_i^\dagger+b_i)|\phi_i\rangle\langle\phi_i|+\sum_i\omega b_i^\dagger b_i \tag{28}$$

Here, the disorder of site energy s_i is assumed to follow a Gaussian distribution $s_i\sim\mathcal{N}(0,\sigma^2)$. The parameters are: vibrational frequency $\omega=1400\,\mathrm{cm}^{-1}$, electron-vibration coupling constant $g=1$, excitonic coupling $J=-100\,\mathrm{meV}$, monomer transition dipole moment $\mu=1$, and temperature $T=300\,\mathrm{K}$. The number of harmonic oscillator basis functions per mode is 7, and time evolution is performed with a 1 fs timestep. The number of electronic states is denoted as N_{mol}. All simulations are performed by the Renormalizer package [41]. In practical calculations of Eq.(27) at each time step, the MPS sites corresponding to the electronic DoFs and the vibrational modes can be reused during MPS-sampling (shown in blue in FIG. 1), while only the auxiliary sites representing the static disorder s_i (shown in red and green) need to be sampled.

First, we compare two types of DVR basis for the auxiliary DoFs: the simple harmonic oscillator DVR (SHODVR) and sine DVR (SineDVR) [35]. SHODVR is expected to have the same accuracy as the bosonic Fock basis used in prior work [17, 19], since only a linear term of s is present in the effective Hamiltonian. The number of DVR basis functions is denoted as N_{b}. Static disorder is continuous and ideally requires an infinite basis set, but in practice, we constrain the SineDVR grids to the range $[-L_{\mathrm{c}},L_{\mathrm{c}}]$ with $L_{\mathrm{c}}=5\sigma$, introducing negligible truncation error (5.74×10^{-7}). For SHODVR, the oscillator frequency is set to $\omega=1/(2\sigma^2)$, aligning the ground-state density with the static disorder distribution. The SineDVR grid points are uniformly spaced: $s_k^{\mathrm{SineDVR}}=-L_{\mathrm{c}}+k\cdot\dfrac{2L_{\mathrm{c}}}{N_{\mathrm{b}}+1}$, while SHODVR grid points are defined via the roots of Hermite polynomial functions: $s_k^{\mathrm{SHODVR}}=\sqrt{2}\sigma\cdot\mathrm{root}_k(H_{N_{\mathrm{b}}}(s))$.

FIG. 2 compares TCFs for a dimer ($N_{\mathrm{mol}}=2$) at $\sigma=50$ and 100 meV, using SHODVR and SineDVR. As expected, both DVRs converge with increasing N_{b}. The static-disorder-averaged TCF decays due to destructive interference across different disorder configurations $\mathbf{s}_k$. However, with finite basis size, artificial Poincaré recurrences emerge. Since recurrence time is inversely related to grid spacing, finer grids delay this artifact. SineDVR outperforms SHODVR, showing later and weaker recurrences with the same grid size, because the SHODVR grid is overly sparse due to the wide spread of basis functions with $\omega=1/(2\sigma^2)$. Therefore, it is preferred to use SineDVR to make the basis size as small as possible for reducing computational cost. In addition, the uniform spacing of SineDVR, $\Delta s=\dfrac{2L_{\mathrm{c}}}{(N_{\mathrm{b}}+1)}$, enables estimating the recurrence time as $T\approx\dfrac{2\pi}{\Delta s}$, which agrees well with numerically observed values (vertical dashed lines in FIG. 2(c, d)). This predictive capability offers a practical advantage that the size of N_{b} can be appropriately chosen according to the required TCF time range. Because of these advantages, SineDVR is recommended for discretizing the auxiliary DoF and is used in all subsequent simulations.

The next key question is whether the auxiliary DoFs significantly increase the MPS bond dimension M, or in other words, whether the total wavefunction $\Psi(t)$ in Eq.(15) is efficiently compressible. The computational cost of TD-DMRG with the projector-splitting time evolution algorithm scales as $\mathcal{O}(M^n)$ with $n\approx2-3$ [42, 43]. If M becomes too large, it would offset the efficiency gains of avoiding multiple independent realizations. FIG. 3(a–c) show TCFs for three random disorder realizations of a 4-site Holstein model, at $\sigma=50$, 100, and 200 meV, respectively. In all cases, a bond dimension of $M=16$ suffices for convergence. FIG. 3(d–f) compare the MPS-sampling method with the direct sampling method (same number of samples, $N_{\mathrm{samp}}=2\times10^4$).

DOI: 10.1063/1674-0068/cjcp2506080 © 2025 Chinese Physical Society

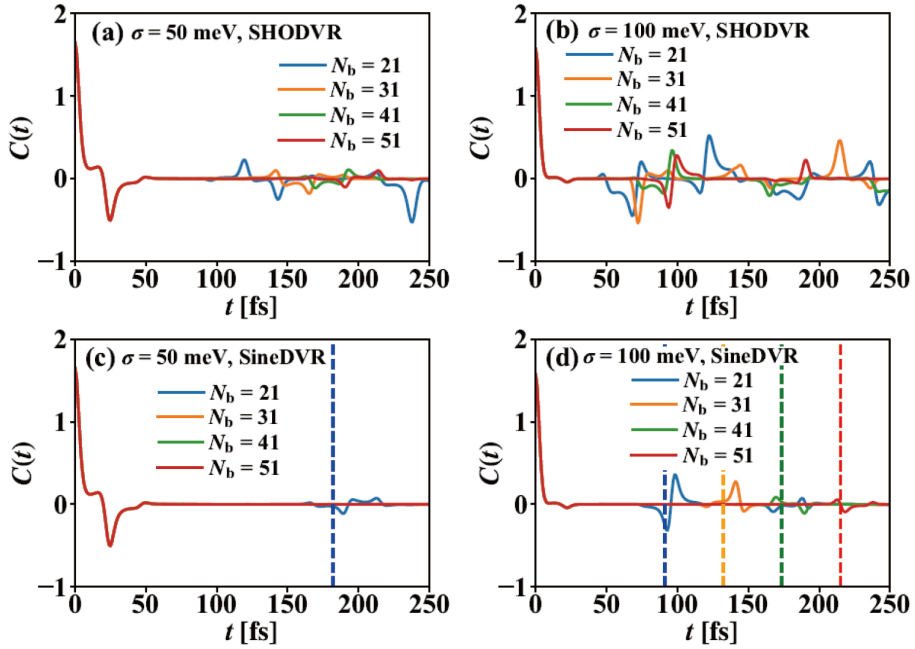

FIG. 2 Real part of the time correlation function $C(t)=\langle\hat{\mu}(t)\hat{\mu}\rangle$ for the emission spectrum of a 2-site Holstein model at 300 K with varying strengths of static disorder (following a Gaussian distribution $\mathcal{N}\sim(0,\sigma^2)$) and two types of DVR grids, computed using the MPS-sampling method ($M=64$, $N_{\mathrm{samp}}=10^6$). (a) $\sigma=50\,\mathrm{meV}$ with SHODVR. (b) $\sigma=100\,\mathrm{meV}$ with SHODVR. (c) $\sigma=50\,\mathrm{meV}$ with SineDVR. (d) $\sigma=100\,\mathrm{meV}$ with SineDVR. Different colors represent different numbers of DVR grid points N_{b}. The vertical dashed line indicates the approximate Poincaré recurrence time, $T=\dfrac{2\pi}{\Delta s}$, for equally spaced SineDVR grids.

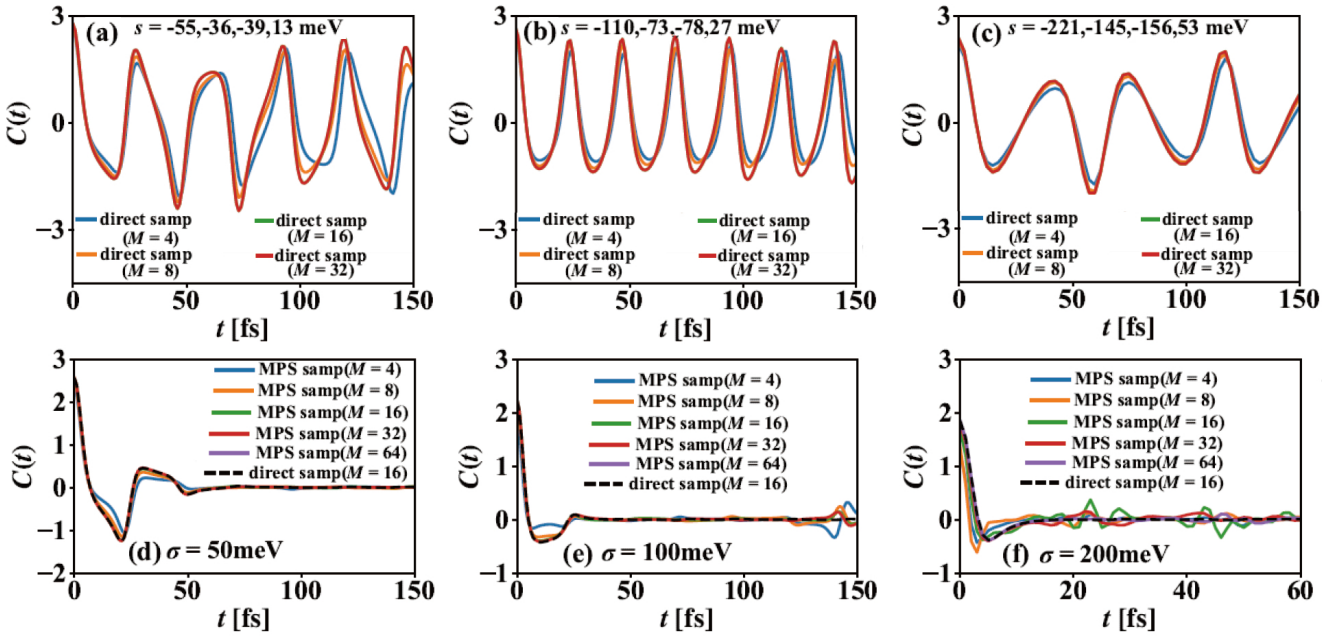

FIG. 3 Real part of the time correlation function $C(t)=\langle\hat{\mu}(t)\hat{\mu}\rangle$ for the emission spectrum of a 4-site Holstein model at 300 K with different bond dimensions M. (a–c) Results from direct sampling for a single realization with $\sigma=50\,\mathrm{meV}$, $100\,\mathrm{meV}$, and $200\,\mathrm{meV}$, respectively. The static disorder values s_i for each site are labeled in the figures. Different colors represent different bond dimensions. (d–f) Results from the MPS-sampling method. The number of DVR grid points is $N_{\mathrm{b}}=21$ for $\sigma=50\,\mathrm{meV}$, and $N_{\mathrm{b}}=31$ for $\sigma=100\,\mathrm{meV}$ and $200\,\mathrm{meV}$. The black dashed lines indicate the reference results from direct sampling. Both methods use $N_{\mathrm{samp}}=2\times10^4$.

The agreement validates the new method. For $\sigma=50$ and $100\,\mathrm{meV}$, the required $M=16$ is similar to that of single realizations, and thus the overall cost reduction is roughly proportional to N_{samp}, since overhead in sam-

DOI: 10.1063/1674-0068/cjcp2506080 © 2025 Chinese Physical Society

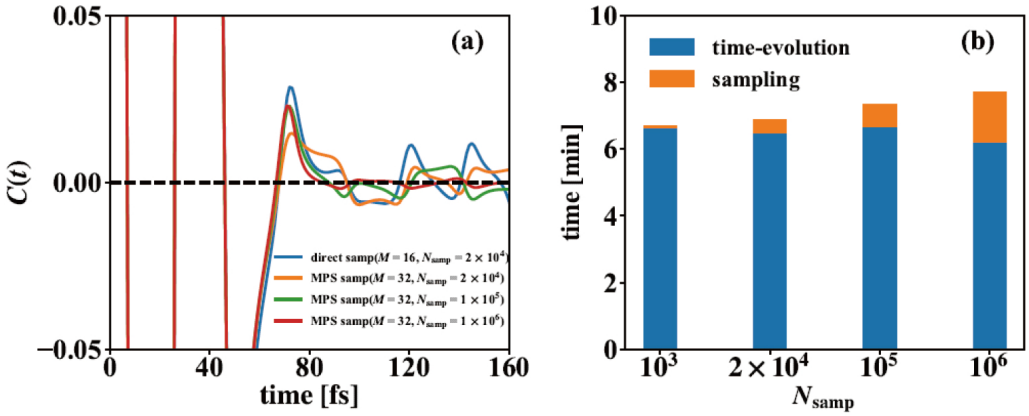

FIG. 4 Real part of the time correlation function $C(t)=\langle\hat{\mu}(t)\hat{\mu}\rangle$ (a) and wall time (b) for computing the emission spectrum of a 4-site Holstein model at 300 K using the MPS-sampling method with varying sample sizes N_{samp}. The static disorder strength is $\sigma=50\,\mathrm{meV}$, and the number of DVR grid points per auxiliary degree of freedom is $N_{\mathrm{b}}=21$. Wall time measurements were performed over 10 time steps using 4 EPYC 7B13 CPU cores and 1 NVIDIA A100 GPU.

pling MPS is cheap due to efficient tensor contractions (see data below). For $\sigma=200\,\mathrm{meV}$, a larger bond dimension (M=64) is required due to greater variation among wavefunctions corresponding to different disorder strengths. As the static disorder strength approaches the electronic bandwidth (approximately 320 meV for the 4-site model with $J=-100\,\mathrm{meV}$), the system undergoes a transition from delocalized to localized states, a phenomenon known as Anderson localization [44]. In this case, compressing both delocalized and localized wavefunctions into a single MPS, as in Eq.(15), becomes inefficient. Therefore, the auxiliary-DoF-based method is most effective when the disorder strength remains smaller than the electronic bandwidth.

Since the MPS-sampling involves efficient tensor contractions and benefits from the reuse of intermediates, it enables much larger sample sizes with minimal overhead than the direct sampling approach to reduce the statistical error. FIG. 4(a) shows reduced noise in the TCF of 4-site model as N_{samp} increases from 2×10^4 to 10^6. The noise increases with evolution time as expected, because at early time, trajectories corresponding to different static disorder realizations remain close, requiring fewer samples to capture the distribution accurately. However, as time progresses, these trajectories diverge due to effects such as chaos, decoherence, or thermalization, leading to increased statistical noise. To compensate for this growing noise, it is better to gradually increase the sample size over time. FIG. 4(b) plots the corresponding wall time for evolving 10 steps. Although the sampling time (*i.e.*, computing the numerator and denominator of Eq.(27)) increases with sample size, it remains a small fraction of the total cost compared to time evolution. As a result, the overall runtime grows only modestly with increasing sample size.

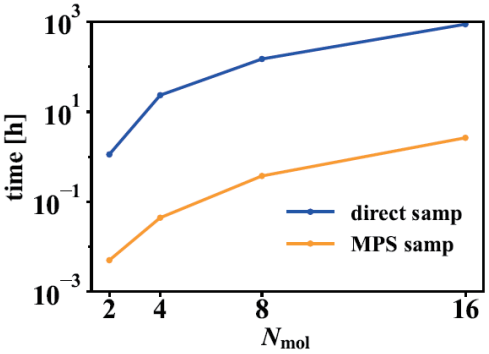

FIG. 5 Wall time for computing the dipole-dipole time correlation function of the Holstein model at 300 K using the MPS-sampling method (yellow) and direct sampling method (blue) for various system sizes N_{mol}. Parameters: $N_{\mathrm{steps}}=10$, $\sigma=50\,\mathrm{meV}$, $N_{\mathrm{b}}=21$, and $N_{\mathrm{samp}}=3000$. Bond dimensions used are: $M=4$ (direct sampling) and $M=8$ (MPS-sampling) for $N_{\mathrm{mol}}=2$; $M=16$ for $N_{\mathrm{mol}}=4$; $M=32$ for $N_{\mathrm{mol}}=8$; and $M=48$ for $N_{\mathrm{mol}}=16$.

FIG. 5 compares the wall time of direct sampling and MPS-sampling methods across various system sizes, using $N_{\mathrm{samp}}=3000$, a typical value for capturing static disorder effects. The bond dimensions used in each converged simulation are listed in the caption. The MPS-sampling method achieves a speedup of about two orders of magnitude, clearly demonstrating its computational advantage, especially as the system size increases.

Finally, we demonstrate that the proposed method is not restricted to Gaussian static disorder, thanks to the use of the DVR basis. As an example, we consider a Lorentzian distribution, which has been used to investigate localization under disorder [15]. The expression of the Lorentzian distribution is as follows:

DOI: 10.1063/1674-0068/cjcp2506080 © 2025 Chinese Physical Society

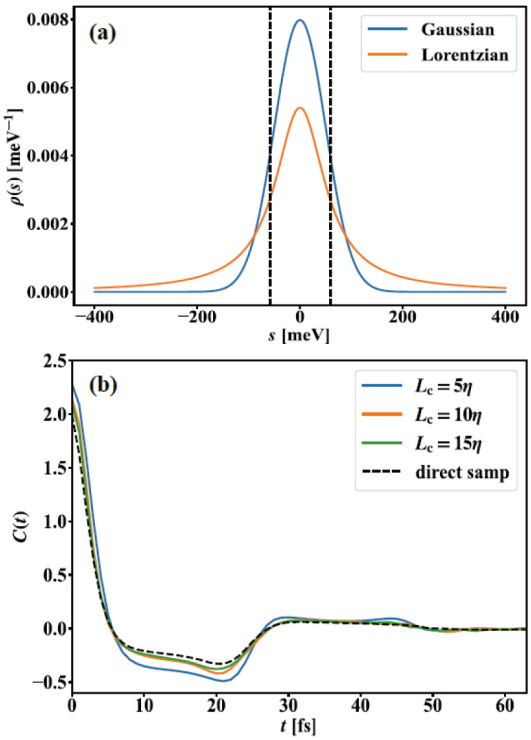

FIG. 6 (a) Comparison of Gaussian distribution with $\sigma = 50\,\text{meV}$ and Lorentzian distribution with $\eta = \sqrt{2\ln 2}\sigma \approx 59\,\text{meV}$, chosen to have the same half width at half maximum, indicated by the vertical dashed line. (b) Real part of the time correlation function for a 4-site Holstein model with static disorder following a Lorentzian distribution ($\eta \approx 59\,\text{meV}$) by the auxiliary degree-of-freedom based MPS-sampling method. Different colors indicate different grid ranges: for $L_c = 5\eta$, grids number $N_b = 21$, bond dimension $M = 16$; for $L_c = 10\eta$, $N_b = 43$, $M = 32$; for $L_c = 15\eta$, $N_b = 31$, $M = 150$. The black dashed line shows the reference result obtained by direct sampling with $N_{\text{samp}} = 2 \times 10^4$, $M = 32$.

$$\rho(s_i) = \frac{1}{\pi} \frac{\eta}{{s_i}^2 + \eta^2}, \tag{29}$$

where η is the parameter to control the width of the distribution. Its heavy-tailed nature, shown in FIG. 6(a), decays more slowly than the Gaussian, requiring a wider DVR grid range to achieve comparable accuracy. To this end, we use SineDVR grids with range cutoff $L_c = 5\eta, 10\eta, 15\eta$, corresponding to truncation errors of 12.6%, 6.3% and 4.2%, respectively (much larger than the Gaussian distribution). For fair comparison with the Gaussian case (σ=50 meV), we choose $\eta = \sqrt{2\ln 2}\,\sigma \approx 59\,\text{meV}$, so that both distributions share the same half-width at half-maximum (HWHM). FIG. 6(b) shows that the TCF converges toward the reference result from direct sampling ($N_{\text{samp}} = 2 \times 10^4$) as the grid range increases. However, a wider grid also leads to larger bond dimensions, since stronger disorder induces greater variation in wavefunctions, through delocalization–localization transitions, making compression more difficult. Although discrepancies remain for the $L_c = 15\eta$ case, the main features of the TCF are well captured. This example highlights that the method is applicable beyond Gaussian disorder, but broader distributions (*e.g.*, with larger variance or longer tails) present increasing challenges for compression.

IV. CONCLUSION

In conclusion, we have developed an MPS-sampling method that extends the auxiliary DoF approach to efficiently treat static-disorder-dependent thermal equilibrium initial states in quantum dynamics simulations. This extension enables the accurate computation of equilibrium time correlation functions in disordered systems through a one-shot simulation, eliminating the need for extensive ensemble averaging.

Our method captures the effects of static disorder with only a moderate increase in the MPS bond dimension compared to conventional direct sampling. It is particularly effective when the disorder strength is smaller than the electronic bandwidth, as demonstrated in benchmarks using the Holstein model. Even for stronger disorder approaching the bandwidth, the required bond dimension increases but remains tractable. We also examined different DVR grid choices for discretizing the auxiliary DoF and found that the SineDVR offers superior convergence and lower recurrence artifacts compared to the harmonic oscillator DVR, making it the preferred basis for practical simulations.

Overall, the MPS-sampling approach offers substantial computational savings, achieving up to a two-order-of-magnitude speedup over traditional methods that require thousands of independent realizations. Furthermore, it enables the efficient generation of very large sample sizes (exceeding 10^6) with minimal additional cost, significantly reducing statistical noise. These advantages make the method a powerful and scalable tool for studying static disorder effects in complex quantum systems.

V. ACKNOWLEDGMENTS

This work is supported by the National Natural Science Foundation of China (No.22273005 and No.22422301), the Innovation Program for Quantum Science and Technology (No.2023ZD0300200), the Na-

DOI: 10.1063/1674-0068/cjcp2506080 © 2025 Chinese Physical Society

tional Security Academic Foundation (No.U2330201), and the Fundamental Research Funds for the Central Universities.

[1] J. M. Moix, M. Khasin, and J. Cao, New J. Phys. **15**, 085010 (2013).
[2] X. Zhong, Y. Zhao, and J. Cao, New J. Phys. **16**, 045009 (2014).
[3] N. J. Hestand and F. C. Spano, Chem. Rev. **118**, 7069 (2018).
[4] X. Peng, Q. Li, and Z. Shuai, Nanoscale **13**, 3252 (2021).
[5] D. Brey and I. Burghardt, J. Phys. Chem. Lett. **15**, 1836 (2024).
[6] J. Zheng, J. Peng, Y. Xie, Y. Long, X. Ning, and Z. Lan, Phys. Chem. Chem. Phys. **22**, 18192 (2020).
[7] Z. Zheng, N. R. Tummala, T. Wang, V. Coropceanu, and J. L. Brédas, Adv. Energy Mater. **9**, 1803926 (2019).
[8] M. L. Chaillet, F. Lengauer, J. Adolphs, F. Muh, A. S. Fokas, D. J. Cole, A. W. Chin, and T. Renger, J. Phys. Chem. Lett. **11**, 10306 (2020).
[9] T. Li, C. Huang, S. Bai, and Q. Shi, J. Chem. Phys. **162**, 094105 (2025).
[10] Z. Zhang, Y. Wang, X. Zheng, J. Ren, Z. Shuai, and W. Fang, J. Phys. Chem. C **129**, 12520 (2025).
[11] H. Bässler, Phys. Status Solidi B **175**, 15 (1993).
[12] S. Jang, S. E. Dempster, and R. J. Silbey, J. Phys. Chem. B **105**, 6655 (2001).
[13] N. Makri, J. Phys. Chem. Lett. **15**, 1462 (2024).
[14] J. Klugkist, V. Malyshev, and J. Knoester, Phys. Rev. Lett. **100**, 216403 (2008).
[15] S. Vlaming, V. Malyshev, and J. Knoester, Phys. Rev. B **79**, 205121 (2009).
[16] A. Eisfeld, S. Vlaming, V. Malyshev, and J. Knoester, Phys. Rev. Lett. **105**, 137402 (2010).
[17] M. F. Gelin, A. Velardo, and R. Borrelli, J. Chem. Phys. **155**, 134102 (2021).
[18] U. Schollwöck, Ann. Phys. **326**, 96 (2011).
[19] Z. Sheng, T. Jiang, W. Li, and Z. Shuai, J. Chem. Theory Comput. **20**, 6470 (2024).
[20] A. Nitzan, *Chemical Dynamics in Condensed Phases: Relaxation, Transfer, and Reactions in Condensed Molecular Systems*, Oxford: Oxford University Press, (2024).
[21] J. Light, I. Hamilton, and J. Lill, J. Chem. Phys. **82**, 1400 (1985).
[22] J. C. Light and T. Carrington Jr., Adv. Chem. Phys. **114**, 263 (2000).
[23] G. Vidal, Phys. Rev. Lett. **93**, 040502 (2004).
[24] A. J. Daley, C. Kollath, U. Schollwöck, and G. Vidal, J. Stat. Mech. Theory Exp. **2004**, P04005 (2004).
[25] A. E. Feiguin and S. R. White, Phys. Rev. B **72**, 020404 (2005).
[26] E. Ronca, Z. Li, C. A. Jimenez-Hoyos, and G. K. L. Chan, J. Chem. Theory Comput. **13**, 5560 (2017).
[27] H. Ma, Z. Luo, and Y. Yao, Mol. Phys. **116**, 854 (2018).
[28] J. Ren, W. Li, T. Jiang, Y. Wang, and Z. Shuai, Wiley Interdiscip. Rev. Comput. Mol. Sci. **12**, e1614 (2022).
[29] H. Ma, U. Schollwöck, and Z. Shuai, *Density Matrix Renormalization Group (DMRG)-Based Approaches in Computational Chemistry*, Amsterdam: Elsevier, (2022).
[30] R. Borrelli and M. F. Gelin, Wiley Interdiscip. Rev. Comput. Mol. Sci. **11**, e1539 (2021).
[31] H. Wang and M. Thoss, J. Chem. Phys. **119**, 1289 (2003).
[32] U. Manthe, J. Chem. Phys. **128**, 164116 (2008).
[33] O. Vendrell and H. D. Meyer, J. Chem. Phys. **134**, 044135 (2011).
[34] H. Wang, J. Phys. Chem. A **119**, 7951 (2015).
[35] M. H. Beck, A. Jäckle, G. A. Worth, and H. D. Meyer, Phys. Rep. **324**, 1 (2000).
[36] A. E. Feiguin and S. R. White, Phys. Rev. B **72**, 220401 (2005).
[37] F. Verstraete, J. J. Garcia-Ripoll, and J. I. Cirac, Phys. Rev. Lett. **93**, 207204 (2004).
[38] T. Holstein, Ann. Phys. **8**, 343 (1959).
[39] W. Li, J. Ren, and Z. Shuai, Nat. Commun. **12**, 4260 (2021).
[40] Z. Shuai, Q. Sun, J. Ren, T. Jiang, and W. Li, Aggregate **6**, e70013 (2025).
[41] *Renormalizer*, https://github.com/shuaigroup/renormalizer.
[42] W. Li, J. Ren, and Z. Shuai, J. Chem. Phys. **152**, 024127 (2020).
[43] J. Haegeman, C. Lubich, I. Oseledets, B. Vandereycken, and F. Verstraete, Phys. Rev. B **94**, 165116 (2016).
[44] P. W. Anderson, Phys. Rev. **109**, 1492 (1958).

DOI: 10.1063/1674-0068/cjcp2506080 © 2025 Chinese Physical Society